CARDIFF UNIVERSITY
PRIFYSGOL CAERDYDD

ORCA – Online Research @ Cardiff

This is an Open Access document downloaded from ORCA, Cardiff University's institutional repository:https://orca.cardiff.ac.uk/id/eprint/95461/

This is the author's version of a work that was submitted to / accepted for publication.

Citation for final published version:

Feng, Q., Tang, Q., Liu, Z., Liu, Ying and Setchi, Rossitza M. 2018. An investigation of the mechanical properties of metallic lattice structures fabricated using selective laser melting. Proceedings of the Institution of Mechanical Engineers, Part B: Journal of Engineering Manufacture 232 (10) , pp. 1719-1730. 10.1177/0954405416668924

Publishers page: http://dx.doi.org/10.1177/0954405416668924

Please note:
Changes made as a result of publishing processes such as copy-editing, formatting and page numbers may not be reflected in this version. For the definitive version of this publication, please refer to the published source. You are advised to consult the publisher's version if you wish to cite this paper.

This version is being made available in accordance with publisher policies. See http://orca.cf.ac.uk/policies.html for usage policies. Copyright and moral rights for publications made available in ORCA are retained by the copyright holders.

An Investigation of the Mechanical Properties of Metallic Lattice Structures Fabricated using Selective Laser Melting

Abstract Metallic lattice structures manufactured using selective laser melting (SLM) are widely used in fields such as the aerospace and automobile industries in order to save material and reduce energy consumption. An essential element of metallic lattice structures design is determining their mechanical behaviors under loading conditions. This paper focuses on the investigation of the mechanical properties of three typical structures fabricated via SLM, and the theoretical analysis of the elastic properties of these three cube-based lattice structures using the force method. The finite element analysis (FEA) and compression experiment study of SLM samples made using Ti6Al4V powders demonstrated the validity of the proposed analytical method.

Keywords: SLM technique, lattice structures, force method, finite element analysis.

1. Introduction

Urgent demands for lightweight material are encouraging the application of metallic lattice structures. Because a lattice structure consists of periodical unit cells, it has a higher ratio of strength to weight as compared with other stochastic lightweight materials, such as metal foam [1]. However, a fabricating metallic lattice structure using conventional processes is time-consuming and impractical when bulk materials with inferior manufacturability, such as titanium alloy, are used. This manufacturing difficulty can be overcome using additive manufacturing (AM). Of the current AM technologies, selective laser melting (SLM) is suitable for fabricating metal parts using various bulk materials. Moreover, due to the high-energy laser beam employed, metal parts fabricated via SLM have high strength and few defects[2]. For example, the density of a titanium part fabricated using SLM can reach 99.9% [3], and its strength can reach up to 1300 MPa [4]. Therefore, lattice structures manufactured using titanium alloy powder provide new business opportunities in sectors such as aerospace and medical implants[5].

Of the many kinds of topologies that can be used in the design of lattice

structures, the body-centred cubic (BCC) lattice structure is very common. Although a BCC structure is not optimal, it has two advantages. First, because low-angle struts should be avoided in order to minimize the warping effect during the SLM process [6,7], the BCC structure can be well-manufactured because the all struts incline properly. Second, the BCC structure has simple deform and failure modes during uniaxial and multiaxial compression [8]. Based on the geometric characteristics of the BCC structure, the mechanical properties of the BCC structure can be calculated efficiently using the beam theory [8]. In order to obtain lattice structures with higher strength, additional struts can be superposed on the BCC unit, and reinforced BCC units can be obtained. Figure 1 shows two types of reinforced BCC structures: BCCZ and f2BCC structures. From the literature we collected, the BCCZ and f2BCC structures have several times the load-bearing capability of the BCC structure, which means that reinforced lattice structures are promising in the lightweight design field [9-11]. However, there are few theoretical studies on the mechanical properties of these reinforced structures manufactured using the current SLM process.

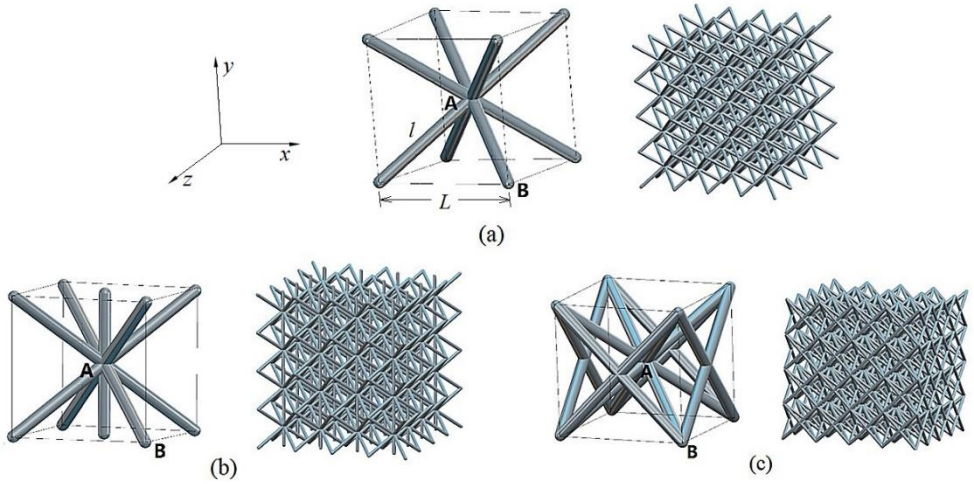

Figure 1. Lattice units and corresponding structures. (a) BCC; (b) BCCZ; (c) f2BCC.

Therefore, this paper describes an extension study of the beam theory used for predicting the mechanical response of metallic lattice structures manufactured using SLM. By utilizing the force method, the mechanical properties of both the BCC and its reinforced structures (BCCZ, f2BCC) can be calculated efficiently and accurately.

The remainder of this paper is structured as follows. The related literature is reviewed in Section 2. Using the force method, theoretical studies of the mechanical properties of BCC, BCCZ and f2BCC structures are conducted in Section 3. Then, compressive sample tests and finite element analysis (FEA) are performed in Section 4. The results, analysis and related discussion will be presented in Section 5. Finally, the conclusions and suggestions for follow-up studies will be listed in Section 6.

2. Related Works

In order to estimate the mechanical response and other multifunctional properties of metallic lattice structures, experimental studies are commonly conducted on samples manufactured using SLM or other similar AM processes. For example, a series of experiments were carried out in order to study the pore size and surface roughness [10], necessary manufacturing process [11], fatigue behavior [12], and flexural properties [13] of lattice structures made using Ti6Al4V. However, because the current SLM process is expensive and time-consuming, analytical study is necessary in order to lower manufacturing costs and the time required.

Early studies of the mechanical properties of metallic lattice structures can be dated to 2001. Using the 'lost wax' investment method, Deshpande et al. fabricated an octet-truss lattice structure made from aluminum alloy. Analytical methods of calculating the stiffness matrix and buckling surfaces of this structure were established, and relevant sample tests were also conducted. The results showed that this structure is stretching-dominated and verified the stretching-dominated criterion [14]. Later, Wallach et al. studied a triangular lattice structure made from aluminum alloy using both experimental and analytical methods, including the numerical relationship between its mechanical properties (elastic modulus and axial and shear strength) and the relative density of the structure. A finite element analysis in which truss elements were used provided results that were in good agreement with the tests and analytical analysis [15]. Common lattice structures that can be manufactured using a conventional process were compared by Wang et al. The Kagome lattice presented good resistance to inner plastic yielding; therefore, the Kagome lattice

showed superior mechanical properties to tetrahedron and pyramid lattices [16].

The lattice structures described above have been fabricated using conventional techniques, which usually demands casting in multiple steps or using a tooled approach [17]. Now, with the application of SLM, metallic lattice structures can be manufactured on a relatively short-time scale, and the size of unit can be on the micrometer scale. Researchers have more design freedom to fabricate structures with curved struts [18]. Unfortunately, limitations resulted from the SLM process should not be ignored. Fabricating parts with low-angle struts demands proper supportive structures [6], and it is impractical to design supportive structures for each inner low-angle strut in lattice structures. Therefore, given this circumstance, low-angle struts should be avoided in lattice structures. Of many kinds of topologies suitable for the SLM process, the BCC structure is commonly a concern for researchers. Based on the homogenous deformation type and the symmetry of the unit, Ushijima et al. proposed a beam-theory-based analytical method to predict the initial stiffness and yield stress of BCC lattice structures [8]. In this method, a force model of a BCC structure under a compressive load can be simplified into a cantilever beam model. By calculating the internal forces and displacements of the free end of the beam, the uniaxial stiffness of the beam can be calculated and deemed the initial stiffness of the entire structure. Using FEA and corresponding compressive tests, the authors found that the experimental data, FEA, and analytical predictions were in good agreement for BCC structures with low relative densities. A similar analytical method was used by Babaee et al. to study the mechanical properties of rhombic dodecahedron lattice structures [19]. Gumruk et al. investigated the compressive response of a BCC lattice structure made in 316L stainless steel. The material overlapping effect near the strut joints was considered when the beam-theory-based method was used; therefore, more reasonable predictions of initial stiffness and yield stresses were obtained [20]. Although the mechanical properties of BCC structures can be improved by increasing their relative densities, they still present relatively lower load-bearing capability because of their bending-dominated properties. Researchers noted that if some struts were added to the BCC unit, the specific stiffness and specific strength of

corresponding structures would be improved significantly. Labeas et al. compared the mechanical properties of BCC structures and BCCZ structures and found that BCCZ exhibited much higher stiffness and buckling load [9]. This phenomenon was also verified by Smith et al. when they proposed the FE modelling of the compressive response of BCC and BCCZ lattice structures. In their project, for BCC and BCCZ lattice structures with the same size (unit volume 2.5 mm^3, strut diameter 0.2mm), the strength of the BCCZ lattice was over six times larger than that of the BCC structure [17].

From the above-mentioned literature, the mechanical properties of BCC structures manufactured via SLM can be predicted accurately using beam theory. However, few studies have been carried out on the BCCZ or f2BCC reinforced structures. The main reason for this is that the additional struts result in complicated and inhomogeneous deformation among struts in each BCCZ or f2BCC unit. Thus, it is difficult to use beam theory to predict the mechanical response of lattice structures with complicated deformation models. Therefore, in order to overcome this problem, the force method will be used in order to carry out theoretical studies of the three structures in the following section.

3. Analytical Method

In order to establish an analytical method of predicting the mechanical response of basic and reinforced structures, three typical lattice structures, i.e., BCC, BCCZ, and f2BCC structures, were analyzed in order to show the validity of this method. As Figure 1 shows, a BCCZ unit is obtained by adding a vertical strut along the Y axis based on the BCC unit, while an f2BCC unit is obtained by adding struts located along the diagonals of four sides of the cube. In this paper, the positive direction of the Y axis is the material stacking direction in the SLM process. Moreover, because this method is based on Euler-Bernoulli beam theory, all struts must be seen as slender beams, and the aspect ratio of strut AB (the ratio of the diameter to the length) in all three structures was set to 0.1.

3.1 Prediction of Mechanical Properties of the BCC structure

Because all struts deform homogeneously when a uniaxial load (along the Y axis in Figure 2) is applied, strut AB was chosen out in order to build a proper force model. Under this loading condition, point A moves vertically, while B moves horizontally with respect to point *o*. Therefore, the force model of Strut AB was established in Figure 2 (b). Note that if the force *q* is born by each unit, then *q/4* is born by each strut.

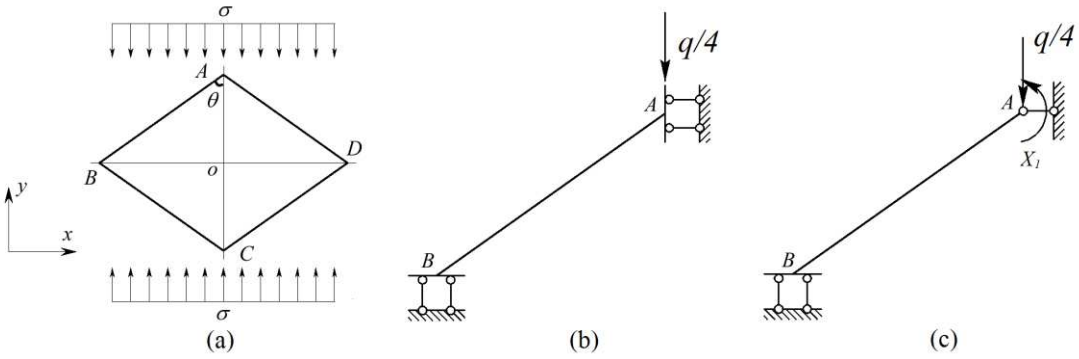

Figure 2. (a) 2D BCC unit under uniaxial loading condition; (b) Force model of strut AB; (c) Fundamental system of strut AB.

Based on beam theory, strut AB can be deemed a beam with one degree of indeterminacy. The corresponding fundamental system of this beam is shown in Figure 2 (c). The additional force X_1 can be obtained using the force method equation:

$$\delta_{ji} X_i + \Delta_{jP} = 0 \quad (1)$$

where X_i is the additional forces, Δ_{jp} represents the displacement in the *j*th direction caused by the external loads, and δ_{ji} represents the unit displacement in the *j*th direction caused by the *i*th additional force.

δ_{ji} and Δ_{jp} can be calculated using Mohr's integrals. The bending moment equation of the strut is therefore proposed as follows:

$$M(x) = \frac{1}{4} q \sin\theta \left(x - \frac{l}{2} \right), \ (0 \le x \le l) \quad (2)$$

The displacement of point A can be obtained via the unit-load method, and the displacement of the BCC unit is twice the displacement of point A:

$$\Delta H = 2\Delta A = 2\int_0^l \frac{M(x)\overline{M}(x)}{EI} dx = \frac{\sigma S l^3 \sin^2\theta}{24EI} \quad (3)$$

where ΔH is the compressional displacement of the BCC unit, E_s represents the elastic modulus of the bulk material, and S is the base area of the design domain of the BCC unit, i.e. the cube.

Force q equals the stress σ multiplied by the base area of the cube S; therefore, the equation for the elastic modulus and geometrical properties of the strut can be obtained:

$$E^* = \frac{\sigma}{\varepsilon} = \frac{48\cos\theta E_s I}{Sl^2 \sin^2\theta} \tag{4}$$

The above equation can be rewritten in the following form:

$$E^* = E_s f_e(\theta)\left(\frac{d}{l}\right)^4 \tag{5}$$

The yield stress of this unit is determined by the plastic hinge formation conditions. According to material mechanics, the bending moment for any section in a beam can be calculated. The force-method-based theoretical method was established, and in the following subsections, this method is used to estimate the elastic properties of two reinforced structures.

3.2 Prediction of Elastic Response of BCCZ Structure

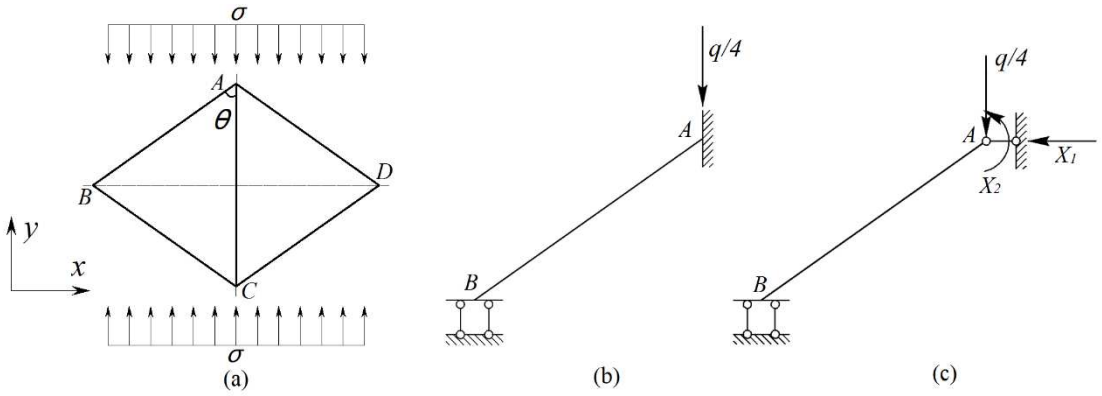

Figure 3. (a) 2D BCCZ unit under uniaxial loading condition; (b) Force model of strut AB; (c) Fundamental system of strut AB.

Because of the vertical struts, the force model for the BCCZ structure is shown in Figure 3 (b). Because point A can be seen as supported by a fixed bearing, the strut AB can be deemed a beam with two degrees of indeterminacy, as shown in Figure 3(c). Based on the force method and using Equation (1), the additional forces X_1 and

X_2 can be calculated. Using the unit load method, the displacement of point A was as follows:

$$\Delta A = 0 \tag{6}$$

Equation (9) shows that the compressive displacement of the BCCZ unit was also 0. This means that the strut AB will deform only if the fixed bearing moves. Because the role of bearing is played by the vertical strut, the elastic modulus of the BCCZ has a superposition relationship:

$$E_{BCCZ} = E_s f_e(\theta)\left(\frac{d}{l}\right)^4 + E_s \frac{\pi d^2}{4L^2} = E_s f_e(\theta)\left(\frac{d}{l}\right)^4 + E_s g(\theta)\left(\frac{d}{l}\right)^2 \tag{7}$$

where l_1 is the length of the vertical strut, the first item in the above equation is the elastic modulus of the BCC structure, and the second item is caused by the additional vertical strut.

3.3 Prediction of Elastic Response of f2BCC Structure

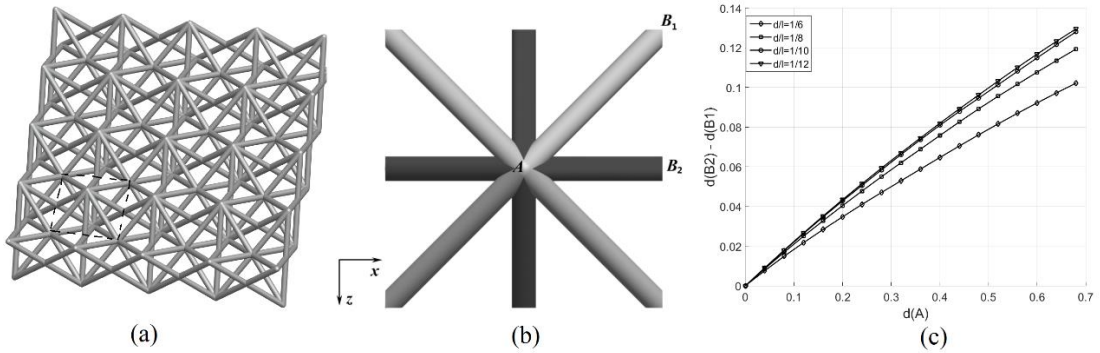

(a) (b) (c)

Figure 4. (a) A layer of f2BCC structure; (b) The f2BCC unit; (c) The difference between the x-axial displacement of Point B_1 and Point B_2.

The basic unit of f2BCC structures is shown in Figure 4(b). It consists of two simple subunits: a BCC unit (lighter color) and a face-centred cubic unit (FCC, darker color). As a result, the f2BCC unit has a more complicated topology. Then, the question becomes how these subunits deform when compressive load along the Y-axis is applied to the entire structure. Therefore, we conducted a previous study on an f2BCC unit using FEA under compressive load along the Y axis. As Figure 4(c) shows, the difference between the displacements of point B2 and point B1 along the X axis were recorded, and units with various strut aspect ratios (the ratio of the

diameter to the thickness of the strut) were analyzed.

As Figure 4(c) shows, an obvious displacement difference of point B_2 and point B_1 along the X axis can be observed, which means that for the f2BCC unit, faster horizontal deformation occurs in the FCC subunit. However, because of the symmetry, strut AB_2 cannot deform freely because it will be squeezed by the adjacent strut in the structure. We then assume that the beam model of strut AB_2 is as shown in Figure 5(a). Strut AB_2 can be deemed a beam with two degrees of indeterminacy.

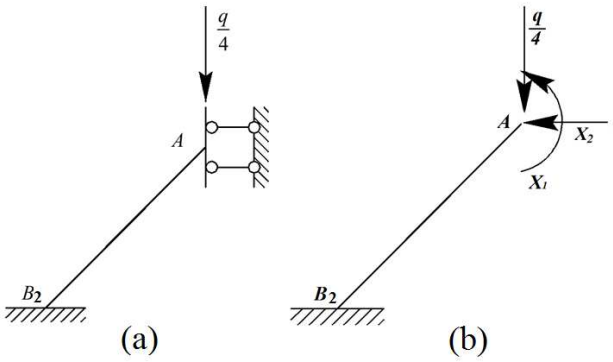

Figure 5. (a) The force model of strut AB_2; (b) Fundamental system of strut AB_2.

Based on the force method and using equation (1), the additional forces X_1 and X_2 can be calculated. Then, the bending moment equation of AB_2 is as follows:

$$M(x)=0,\ (0\le x\le l) \tag{8}.$$

Equation (11) shows that there is only axial force on strut AB_2, which means that the FCC subunit is stretching-dominated. Using the energy principle yields the following:

$$q\Delta H=\sum_i \frac{1}{2}\frac{(F_i)^2 l_i}{E_i A_i} \tag{9}$$

where F_i, l_i, E_i, and A_i are the axial force, length, elastic modulus, and area of the cross-section of the ith strut, respectively.

From Equation (12), the compressive displacement of the FCC subunit can be obtained, and its elastic modulus can be calculated as follows:

$$E_{FCC\_S}=E_s\frac{\pi\cos^3\theta_2}{4\sin^2\theta_2}\left(\frac{d}{l_2}\right)^2=E_s h(\theta_2)\left(\frac{d}{l}\right)^2 \tag{10}$$

where l_2 is the length of the strut AB_2.

Then, the initial stiffness of the f2BCC structure can be calculated as follows:

$$E_{f2BCC} = E_s f_e(\theta_1)\left(\frac{d}{l}\right)^4 + E_s h(\theta_2)\left(\frac{d}{l}\right)^2 \tag{11}$$

Equations (5), (7), and (11) reveal that there are exponential relationships between the elastic property and the geometrical factors of the three structures. Moreover, there is only a fourth-power term in Equation (5), while additional square terms exist in Equations (7) and (11) as a consequence of additional struts. Therefore, the stiffness of BCCZ and f2BCC structures will be improved significantly as compared with the basic BCC structure according to the theoretical methods. In Section 4, an experimental study and FEA will be carried out in order to verify this conclusion.

4. Experimental Study and FEA

In order to verify the theoretical method proposed in Section 3, an experimental study and FEA were carried out in this section. First, uniaxial compression tests were conducted on Ti6Al4V samples fabricated using the three above-mentioned types of lattice structures. In this step, the engineering stress-strain diagrams can be obtained, and the experimental data should be correlated with theoretical predictions. Then, FEA was carried out in the following step to illustrate the stress distribution and deformation type of the three structures under uniaxial loading conditions.

4.1 Equipment, Material, and Samples

The equipment used for fabricating these samples is an EOS M280 SLM system located in the Additive Manufacturing Research Center of Chongqing University, China. The effective build volume is 250 mm × 250 mm × 325 mm. The powders used for fabricating the samples were made using Ti6Al4V. A previous study on powder morphology showed that the maximun diameter of powders is around 30 μm.

As Figure 6 (a) shows, all samples are made as cubic blocks, and their size is 24mm×24mm×24mm. I.e., there are four cubic units on each edge. As mentioned above, the analytical method proposed in this paper is based on Euler-Bernoulli beam

theory, which demands that the beam be slender. Therefore, the diameter-to-length ratio of each strut is determined to be 0.1. Then, the diameter of each strut is around 0.52mm. CAD models of the structures were transformed into stl files, which were imported into the EOS machine. Then, the samples were manufactured layer-by-layer in terms of corresponding 2d images of cross-sections. During the manufacturing process, the laser power was 200 w, the scan speed was 1,600 mm/s, the layer thickness was 30 um, the hatching space was 0.1mm, and diameter of the laser spot was 0.1mm.

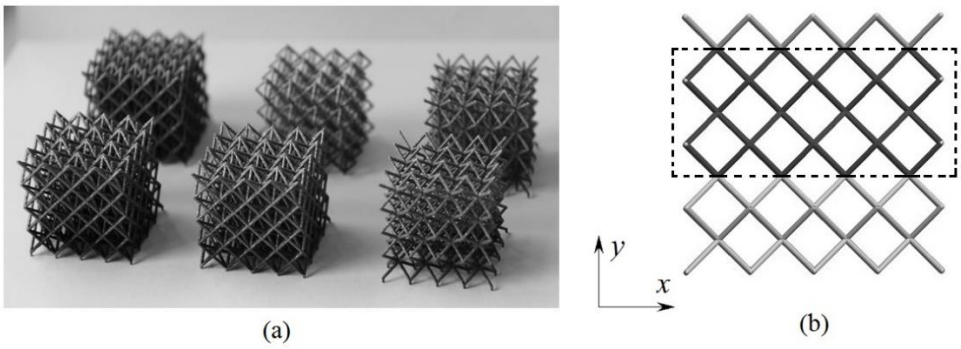

Figure 6. (a) Samples of Ti6Al4V structures; (b) The elevation view of the BCC structure.

A series of uniaxial compressive tests were carried out on a universal test machine. These lattice samples were loaded in the build direction during SLM, namely the Y axis direction. The displacement rates of the crosshead were properly set. Therefore, the strain speed was 0.005 per minute in each test (ASTM standards). The displacement and reaction force of the crosshead were recorded during each compression test in order to plot the engineering stress-strain diagrams.

4.2 Finite Element Analysis

In order to analyze the stress distribution and deformation properties of the aforementioned lattice structures, FEA was carried out to simulate the uniaxial compression tests using ABAQUS commercial finite element software.

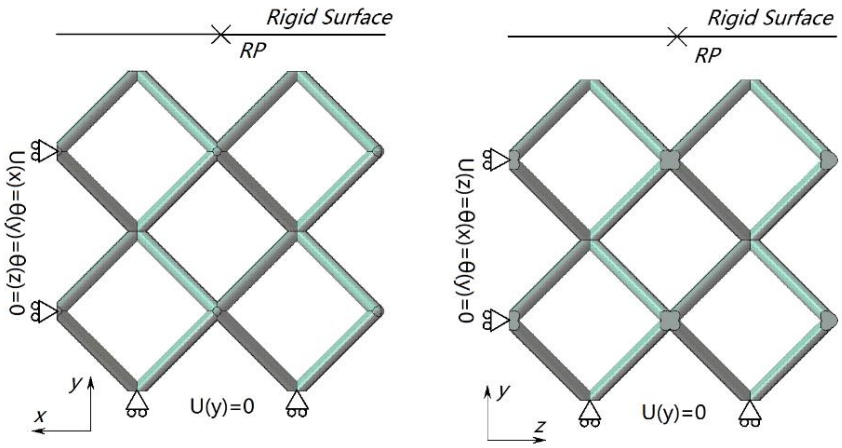

Figure 7. Boundary conditions for BCC structures.

For the BCC structure, the simulation approach called the continuum elements model was carried out. In order to reduce the computation time, two layers of the BCC structure were chosen (the darker layers shown in Figure 6.b). Moreover, the two-layer-model can show the interaction between adjacent units under compressive loading conditions. Figure 7 shows the continuum model of the BCC structure. Because of the symmetry, one-quarter of the two-layer structure was chosen for use as the FE model. Therefore, corresponding symmetry conditions were established. For the BCCZ and f2BCC structures, the continuum element models were also used. The boundary conditions were similar to those used in the BCC model.

In all three FE models, analytical rigid surfaces were built and used as the crosshead in compression tests. Rigid and non-friction contact conditions were set between the rigid surface and the top surface of the structures. A reference point (PR in Figure 7) placed at the center of the surface has two functions: one is to apply the displacement boundary conditions to the models, and the other is to record the displacements and reaction forces from the structures in order to draw the engineering stress-strain curves. Two steps were established for each FE model after the default initial step. The first step was called ‘InContact’, in which the rigid surfaces would move downward properly and create the non-frictional contact relationship between the rigid surfaces and the structures. Then, the rigid surfaces compressed the structures in the next step, called ‘Press’. Moreover, all material models are assumed

to be isotropic, and the Mises yield criterion was used in the FEA analysis. Because the process parameters are similar to those in a previous work [4], the material was set to Ti6Al4V, whose elastic modulus is 110 GPa and yield strength is 1110 MPa. When the stress reaches up to 1270 MPa, the strain is 0.02.

5 Results and Discussion

In order to analyze the validation of the theoretical method proposed in Section 3, the engineering stress-strain curves based on the results obtained from the theoretical methods, FEA, and sample tests are depicted in Figures 8-10. Here, the bulk material properties used in the theoretical equations are similar to those in the FEA, which means that its elastic modulus E_s is 110 GPa and yield strength σ_s is 1100 MPa.

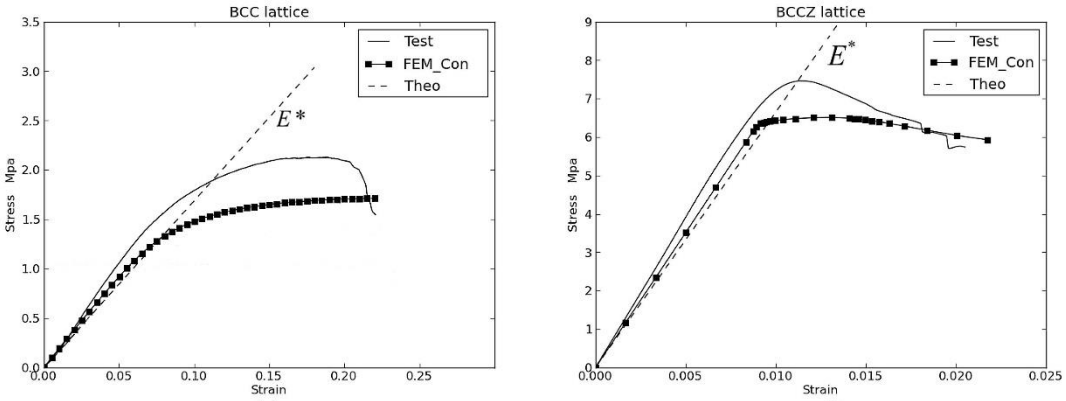

Figure 8. Stress-strain curves of the BCC (a) and BCCZ structures (b).

Figure 8 (a) shows the engineering stress-strain curves for the BCC structure based on the results of the theoretical analysis, FEA, and uniaxial compression tests. The box line represents the results from the continuum elements method, while the spot line represents the results from the beam element method. The line in this figure shows the elastic modulus obtained via Equation (5). For the BCC structure, the theoretical results are 16.88 MPa for elastic modulus E^*, while those from the continuum elements method are around 20 Mpa and 1.5 MPa, which are slightly bigger than the analytical predictions. The testing result shows that the elastic modulus and yield stress are around 24 MPa and 1.7 MPa, respectively.

From Figure 8 (a), the reasonable mechanical properties of a BCC structure

manufactured using SLM can be calculated via the force method proposed in Section 3. However, we need to discuss the discrepancies between the theoretical analysis, FEA, and experimental study. During the elastic stage, the results obtained via theoretical analysis were smaller than the results obtained using the FEA and compression test. The main reason is that the overlapping effect in the joints of the strut was not taken into account. Therefore, the actual length of each strut is relatively smaller. Based on Equation (5), with its the four-fold power relationships, using the theoretical methods will lead to smaller results. This effect can be tackled using the calculation method for effective strut length proposed by Gümrük et al. [20]. In this way, more reasonable results that are closer to the experimental data can be obtained.

Figure 8 (b) shows the engineering stress-strain curves obtained for the BCCZ structures. The elastic modules from the theoretical analysis, FEA, and experimental study are around 665 MPa, 712MPa, and 775 MPa, respectively. Therefore, the validation of Equation (7) based on the force method can be verified by both FEA and the experimental study. Moving from the BCC structure to the BCCZ structure, the elastic modulus is increased from around 20MPa to around 700MPa, as shown in Figure 9 (b). Therefore, the vertical strut becomes the main load-bearing strut in the BCCZ unit. From both Figure 8 (a) and (b), we can see that the results from the compression tests are higher than those from the FEA and theoretical analysis. The deviations in these results are caused by the SLM process. Firstly, the rapid melting and cooling of bulk material causes residual stress in structures, which affects the experimental data and causes the deviation. Secondly, partially melting powders will attach to the strut, which causes the variation of the diameter of strut, while strut diameter is constant in the FEA and theoretical studies.

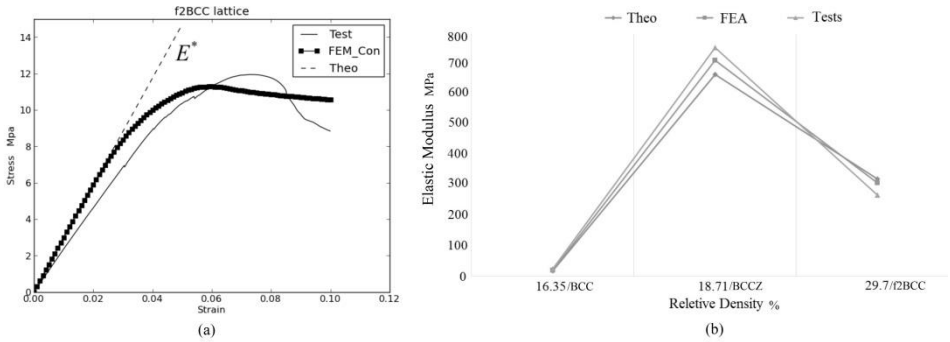

Figure 9. (a) Stress-strain curves of the f2BCC structure; (b) Comparison of the three structures.

Figure 9 (a) shows the engineering stress-strain curves of the f2BCCZ structures. The elastic modules from the theoretical analysis, FEA, and experimental study are around 321MPa, 307MPa, and 268 MPa, respectively, and these results are in good agreement. Therefore, the force method proposed in Section 3.3 can properly estimate the elastic properties of complicated f2BCC structures. Moving from the BCC structure to the f2BCC structure, the elastic modulus is increased from around 20MPa to around 300MPa, as shown in Figure 9 (b), and this change is caused by the fact that the FCC subunit becomes the main load-bearing part based on the assumption in Section 3.3. Because the theoretical analysis has given a reasonable result compared with the FEA and experimental study, we can confirm that the assumption in which the FCC subunit is stretching-dominated under a compressive loading is reasonable because the ratio of the strut diameter to strut length is small and the strut can be seen as a slender beam. Another important phenomenon is that the theoretical result is larger than both the FEA and experimental data. This phenomenon is caused by the beam model used in Section 3.3. Because point B_2 is fixed in Figure 5, the strut AB_2 contains only axial force. However, point B_2 moves horizontally due to the movement of the whole unit, which has not been taken into account by the beam-based force model in Figure 5, and therefore, Equation (11) is an approximate equation. To obtain a more accurate equation, the accurate deformation type of strut AB' should be studied in the future.

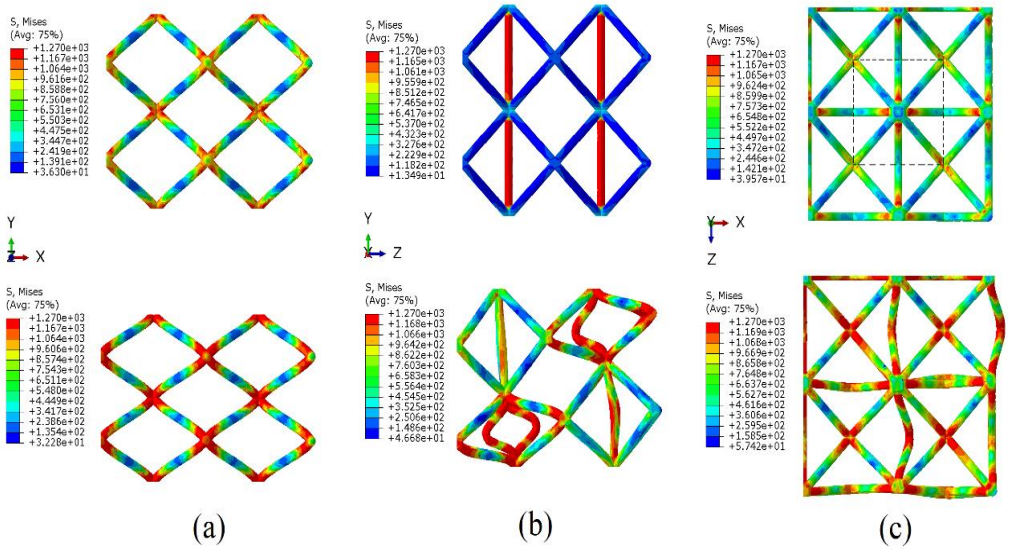

Figure 10. Stresses distribution and deformation of the structures: (a) BCC; (b) BCCZ; (c) f2BCC. Compression loads were applied along the Y axis.

Figure 10 shows the stresses distribution and deformation of BCC, BCCZ, and f2BCC structures under uniaxial compression loading conditions, obtained by FEA. The first row in this figure shows the situations in which the three structures began to yield under compression loading along the Y axis. The second row shows the situation when the compressive process ended. The left column (Figure 10.a) shows the BCC structure during the compressive process. We can see that during the whole compressive process, the deformation of the BCC structure is homogenous within the scale of the struts, and the stress distribution in each strut is nearly the same as in the elastic or plastic stage. This is the reason why only one strut can be analyzed in order to estimate the properties of the entire BCC structure. Moreover, when the BCC structure began to yield, the highest-stress zones were located in the vicinity of strut nodes, where the limit bending moment of each strut took place. The middle column (Figure 10.b) shows the situation when the BCCZ structure was under uniaxial loading conditions. We can confirm that the vertical struts are the main loading-bearing struts because when the material in the vertical struts started to yield (the Mises stress in the vertical struts exceeded 1100MPa), the highest stresses in the other struts were only around 200MPa. When the vertical struts buckle, the $45°$ shear band can be seen in Figure 10 and in compression experiments on BCCZ structures

conducted by Smith et al. [17]. The right column (Figure 10.c) illustrates the situation when the f2BCC structure was under uniaxial loading conditions. When the structure began to yield, the highest-stress zones were located in the vicinity of nodes where the struts of BCC subunits and FCC subunits intersected (the f2BCC unit is shown in the dashed-line square in Figure 10.c). Moreover, the highest-stress zones were located in struts of the FCC subunits. The final deformation of the f2BCC structure shows that the struts of the FCC subunits buckled, while the struts of the BCC subunits illustrate homogenous stress distribution and deformation. Because buckling is caused by axial forces, this phenomenon correlates with the assumption proposed in the theoretical analysis: the struts of FCC subunits bear mainly axial forces.

From the above discussion, predictions of the mechanical properties of BCC, BCCZ, and f2BCC structures made using theoretical equations based on the force method were verified by both FEA and compression experiments. However, further studies should be carried out. First, the plastic properties of the three structures should be studied. Unlike a BCC structure, which has a simple failure mode, the two reinforced structures have more complicated yield criteria because of the additional struts. Therefore, the failure modes of BCCZ and f2BCC will be complicated. Second, in this paper, all struts in these structures can be deemed slender beams. Therefore, for the structures with larger strut aspect ratios, more comparative FEA and experimental studies need to be carried out in order to validate and modify the theoretical equations proposed in this paper. Third, the SLM process parameters and heat treatment procedures were not taken into account. Corresponding effects should be considered in order to evaluate the mechanical properties of these structures fabricated by the SLM process more accurately.

6. Concluding Remarks

This paper presents a force-method-based analytical method for predicting the mechanical properties of BCC structures and reinforced BCCZ and f2BCC structures fabricated using the current SLM process. Although the mechanical properties of the BCC structure can be predicted accurately using the current beam-method-based

theoretical method, it is difficult to predict the mechanical properties of the reinforced structures because their inner struts do not deform homogenously, because of the additional struts. This difficulty was overcome via the analytical approach based on the force method, using the following steps. First, the force model of the basic BCC structure under compression loading was simplified to a beam with one degree of indetermination. Then, the mechanical properties were calculated. When additional struts were added to the BCC unit, the force model of the corresponding BCCZ or f2BCCZ structures was simplified to different beams with two degrees of indetermination. Then, their elastic properties were predicted. Because the mechanical properties of these structures were predicted by theoretical analysis and the validity of this method was verified via FEA and compression tests on SLM samples, the theoretical analysis proposed in this paper was deemed a useful and reasonable approach to evaluating the mechanical properties of BCC and its reinforced structures.

Because all the struts in these structures were thought of as slender beams and manufacturing effects were not taken into account, further studies should be carried out, and more FEA and sample experiments on these structures with various strut aspect ratios are needed. The plastic properties of the BCCZ and f2BCC structures, the effects of the SLM process, as well as the appropriate heat treatment measures to use in eliminating residual stresses in these structures will be examined in future research.

Acknowledgments

This study was supported by the National Science Foundation of China (No: 51405046). Sincere thanks are expressed to the Additive Manufacturing Research Center of Chongqing University (China) for the manufacturing and testing of the Ti6Al4V samples.

References

1. Kooistra GW, Deshpande VS, and Wadley HNG. Compressive behavior of age hardenable tetrahedral lattice truss structures made from aluminium. *Acta Mater 2004;* 52(14): 4229–4237.
2. Yan C, Hao L, Hussein A, et al. Advanced lightweight 316L stainless steel cellular lattice structures fabricated via selective laser melting. *Mater. Des.* 2014; 55: 533–541.
3. Kong C, Tuck CJ, Ashcroft IA, et al. High density Ti6Al4V via SLM processing: microstructure and mechanical properties. In: *SFF* 2011; 475–483.
4. Vrancken B, Thijs L, Kruth JP, et al. Heat treatment of Ti6Al4V produced by Selective Laser Melting: Microstructure and mechanical properties. *J. Alloys Compd.2012;* 541: 177–185.
5. Amin Yavari S, Ahmadi SM, van der Stok J, et al. Effects of bio-functionalizing surface treatments on the mechanical behavior of open porous titanium biomaterials. *J. Mech. Behav. Biomed. Mater.*2014; 36: 109–119.
6. Kim TB, Yue S, Zhang Z, et al. Additive manufactured porous titanium structures: Through-process quantification of pore and strut networks. *J. Mater. Process. Technol.*2014; 214(11): 2706–2715.
7. Hussein A, Hao L, Yan C, et al. Advanced lattice support structures for metal additive manufacturing. *J. Mater. Process. Technol.2013;* 213(7): 1019–1026.
8. Ushijima K, Cantwell W, Mines R, et al. An investigation into the compressive properties of stainless steel micro-lattice structures. *J. Sandw. Struct. Mater.2011;* 13(3): 303–329.
9. Labeas GN and Sunaric MM. Investigation on the static response and failure process of metallic open lattice cellular structures. *Strain* 2010; 46(2): 195–204.
10. Parthasarathy J, Starly B, Raman S, et al. Mechanical evaluation of porous titanium (Ti6Al4V) structures with electron beam melting (EBM). *J. Mech. Behav. Biomed. Mater.2010;* 3(3): 249–259.
11. Pattanayak DK, Fukuda A, Matsushita T, et al. Bioactive Ti metal analogous to human cancellous bone: Fabrication by selective laser melting and chemical treatments. *Acta Biomater.2011;* 7(3): 1398–1405.
12. Amin Yavari S, Wauthle R, Van Der Stok J, et al. Fatigue behavior of porous biomaterials manufactured using selective laser melting. *Mater. Sci. Eng. C 2013;* 33(8): 4849–4858.
13. Horn TJ, Harrysson OLA, Marcellin-Little DJ, et al. Flexural properties of Ti6Al4V rhombic dodecahedron open cellular structures fabricated with electron beam melting. *Addit. Manuf.2014;* 1–4: 2–11.
14. Deshpande VS, Fleck NA, and Ashby MF. Effective properties of the octet-truss lattice material. *J. Mech. Phys. Solids 2001;* 49(8): 1747–1769.
15. Wallach JC and Gibson LJ. Mechanical behavior of a three dimensional truss material. *Int. J. Solids.struct.2001;* 38(40–41): 7181–7196.

16. Wang J, Evans AG, Dharmasena K, et al. On the performance of truss panels with Kagome cores. *Int. J. Solids Struct.2003;* 40(25): 6981–6988.
17. Smith M, Guan Z, and Cantwell WJ. Finite element modelling of the compressive response of lattice structures manufactured using the selective laser melting technique. *Int. J. Mech. Sci.* 2013; 67: 28–41.
18. Yan C, Hao L, Hussein A, et al. Evaluations of cellular lattice structures manufactured using selective laser melting. *Int. J. Mach. Tools Manuf.* 2012; 62: 32–38.
19. Babaee S, Jahromi BH, Ajdari A, et al. Mechanical properties of open-cell rhombic dodecahedron cellular structures. *Acta Mater.2012*; 60(6–7): 2873–2885.
20. Gümrük R and Mines RAW. Compressive behaviour of stainless steel micro-lattice structures. *Int. J. Mech. Sci.2013*; 68: 125–139.